Desalination and Water Treatment
www.deswater.com

doi:10.5004/dwt.2019.24056

153 (2019) 234–243
June

Synthesis and characterization of versatile MgO: synthetic wastewater treatment and anti-bacterial activity against *B. subtilus* and *E. coli*

N.S. Awwad[a,*], I.S. Yahia[b], A.E. AL-Salami[c], M.S. Hamdy[a], H.A. Ebrahium[c,d]

[a]*Department of Chemistry, Faculty of Science, King Khalid University, P.O. Box 9004, Abha, Saudi Arabia, Mobile: +966-563764476, email: aawwad@kku.edu.sa (N.S. Awwad), m.s.hamdy@gmail.com (M.S. Hamdy)*
[b]*Department of Physics, Faculty of Science, King Khalid University, P.O. Box 9004, Abha, Saudi Arabia, email: dr_isyahia@yahoo.com (I.S. Yahia), aeslami@kku.edu.sa (A.E. AL-Salami)*
[c]*Department of Chemistry, Faculty of Girl Science, King Khalid University, P.O. Box 9004, Abha, Saudi Arabia, email: halaalyhend@yahoo.com (H.A. Ebrahium)*
[d]*Department of Biology, Nuclear Materials Authority, P.O. Box 530, El Maadi, Egypt*

Received 29 September 2018; Accepted 1 March 2019

ABSTRACT

The removal of bromophenol blue dye from textile wastewater effluents using nano-crystalline magnesium oxide (MgO) was studied. Nano MgO was prepared by a co-precipitation method. The parameters that affected the dye uptake, contact time, reagent dosage and pH were examined and optimized. The dye adsorption equilibrium data fit well to the Langmiur isotherm, but not to the Freundlich isotherm. The adsorption isotherm indicates that the adsorption capacity was 124 mg of dye per gram of MgO. The adsorption isotherms, including the Langmuir constant (*Q* degrees and *b*) and Freundlich constant (*K(F)* and *n*) for the dye, decreased with an increase in temperature. The value of enthalpy change (ΔH) for bromophenol blue dye was –56.5 kJ/mol, indicating that the removal process is exothermic. The adsorption of the dye was enhanced by increasing the pH, reaching a maximum at pH 6–11. MgO was also used because of its antibacterial activity against *B. subtilus* and *E. coli*, and we found that the best inhibitory parameters for MgO nanoparticles against 10^8 CFU/ML of *B. subtilus* and *E. coli* were 0.5 gm of MgO and 4 h to kill all cells, as shown in the TEM images. MgO was characterized by X-ray diffraction (XRD), atomic force microscopy (AFM) and diffuse reflectance spectroscopy (DR) before and after the removal of bromophenol blue.

Keywords: Nano-crystalline MgO; Bromophenol blue dye; Wastewater treatment; Optical spectroscopy; Atomic force microscopy; TEM

1. Introduction

According to the Society of Dyers and Colorists and the American Association of Textile Chemists and Colorists, data reported for the Color Index (C.I.) approximately equals 10,000 different types of synthesized dyes. The available data about the production of dyes also annually equals 700,000 tons, as reported in the literature [1,2]. Clearly, there is a large amount of dye waste that affects our land and even more wastewater that affects plants, animals and human health and life. The textile and other industries generate a number of visual pollutants, which they discharge to the surrounding environment without any further treatment. These pollutants not only add colour to water but also cause extensive toxicity to aquatic and other forms of life. Approximately 10–15% of the total dyes from various textile and other industries become discharged in wastewater and cause extensive pollution [3]. Therefore, the treatment of industrial effluents containing aromatic compounds becomes necessary prior to their final discharge to the environment. Many papers have reported methods for dye removal from wastewater by applying different methods, including biological processes, combined chemical

*Corresponding author.

and biochemical processes, chemical oxidation, adsorption, coagulation and membrane treatments; each of these has specific advantages and disadvantages [4]. Recently, adsorption has been one of the most used techniques for dye removal. This is likely because of its simplicity and high level of effectiveness [5]. Nano-crystalline metal oxides, in particular magnesium oxide (MgO), have promising applications as adsorbents in wastewater treatment because of their low production cost, environmental impact and because they are essential for plant, animal, and human life. The advantages of MgO can be summarized as follows: (i) its large specific surface area and high surface reactivity due to its nano-scale and (ii) its ability to be prepared from readily available and economical precursors [6–9]. Additionally, the efficient removal of various pollutants has been found when nano-MgO has been utilized [6,7]. In addition, nano MgO has a good bactericidal performance in aquatic environments. Recently, it was reported [10,11] that MgO has good bactericidal performance in aqueous environments because of the formation of superoxide (O^{2-}) anions on its surface. Klabunde, Marchin and co-workers [12,13] demonstrated that nano-MgO exhibits a high activity against bacteria, spores and viruses after the adsorption of halogen gases because of its large surface area, abundant crystal defects and positively charged particles, which can result in strong interactions with negatively charged bacteria and spores. Many nano-sized inorganic metal oxides degrade chemical warfare agents or their surrogates in heterogeneous catalysis: CaO [14], Al_2O_3 [15,16], MgO [16], TiO_2, Al_2O_3/CuO [17], ZnO [18], TiO_2, ZnO, Al_2O_3 [19], CuO/ZnO [20], Al_2O_3, MgO, ZnO, CeO_2, CuO, and TiO_2 [21,22]. Among these compounds, magnesium oxide (MgO) is one of the most frequently used [23–25]. Some of these oxides have been tested against microbes, such as bacteria or viruses, which may also be agents of the threat: ZnO against *Escherichia coli* [26], ZnO, MgO, Zn/MgO against *Bacillus subtilis* and *E. coli* [27], MgO, CaO, MgO/Cl_2, MgO/Br_2 against *E. coli, Bacillus sp.* and a *virus* [28], MgO against *Staphylococcus* and *E. coli* [29]. According to these published studies, magnesium oxide seems to be able to neutralize both toxics and biological agents. As magnesium oxide is a nontoxic, environmentally friendly and low-cost material, the ability of this component to act both on chemicals and microbes makes it a promising reagent to be included in a broad spectrum decontamination system. *E. coli* is the most common foodborne pathogens responsible for millions of cases of illnesses and hundreds of deaths each year in the United States. *B. subtilis* is a kind of spore with a compact cell wall that has strong resistance again chemical agents [30]. Bromophenol blue dye is used as a colour marker to monitor the process of agarose gel electrophoresis and polyacrylamide gel electrophoresis. In addition, it is used as an acid-base indicator,may cause respiratory tract irritation, may be harmful if absorbed through skin, may cause skin irritation and may cause eye irritation. The removal of bromophenol blue dye by the sequencing batch technique was investigated in this study.

This study investigated the use of MgO for two separate applications: 1) the removal of the bromophenol blue dye as an organic pollutant from synthetic wastewater and 2) the use of MgO antibacterial activity against *B. subtilus* and *E. coli* in synthetic wastewater.

2. Experimental procedures

2.1. Preparation of nano-crystalline MgO powders

All chemicals were purchased from Sigma-Aldrich without further purification. MgO were prepared by a co-precipitation method as follows: 2 M $MgCl_2{\cdot}2H_2O$ and NaOH were dissolved in deionized water at 50°C in separate beakers for 1 h to produce transparent, clear solutions. After complete dissolving of $MgCl_2{\cdot}2H_2O$, NaOH was added drop wise until the clear solution became a white precipitate. The white precipitate was stirred for another one hour to complete the reaction. The precipitate was collected by filtration, washed with deionized water several times, and then wash with ethanol in a last stage. After washing, the final product was dried at 150°C for 2 h. The dried powder was inserted in a high temperature furnace for calcinations at approximately 500°C for 3 h to remove any organic residuals inside the nano-powder [31].

2.2. Bactericidal testing

After the MgO was heated at 120°C for 20 min, 0.5 g samples of MgO were placed in a sterile conical flask, and 50 ml of phosphate buffer was added (pH 6.8) followed by 0.5 ml of *Bacillus subtilis* and *E. coli* (10^8 cfu/ml). The sample was mechanically shaken at specific time intervals (0, 0.5, 1, 2, 4, and 6 h) at 37°C, and an aliquot (0.5 ml) of the liquid mixture was placed on a sterile plate with a general germ culture medium and cultured for 24 h at 37°C. The surviving colonies were counted by eye. The tests were conducted at least three times with each MgO sample including both *B. subtilis* and *E. coli*, and the average CFU/ml (log 10) were calculated as shown in Table 1.

2.2. Measurements

A fully automated NT-MDT SOLVER NEXT Atomic force microscope (AFM) was used for scanning the nano-crystalline MgO in semi-contact mode.

X-ray diffraction patterns were conducted by an XRD-6100 X-ray diffractometer with *CuK*α (λ = 1.5406 Å) radiation in the 2θ range from 5 to 90°. The scanning mode was continuous with a scan speed of 2 deg/min; the sampling pitch was 0.02 deg, and the preset time was 0.6 s.

Table 1
Antimicrobial effect of MgO against of *B. subtilis* and *E. coli* (10^8 cfu/ml), at different times. Control sample is *B. subtilis* and *E. coli* without MgO

Time (h)	Average number of CFU/ml *B. subtilus*		Average number of CFU/ml *E. coli*	
	Control	With MgO	Control	With MgO
0	8	8	8	7
0.5	8	6	8	6
1	8	4	8	3
2	8	2	8	1
4	7	0	8	0
6	7	0	7	0

For diffuse reflectance (DR) measurements, a Shimadzu UV-VIS-NIR spectrophotometer (UV-3600) was used to measure the DR in the wavelength range of 230–800 nm using integrating sphere attachments and $BaSO_4$ as the reference.

2.3. Adsorption studies

Adsorption equilibrium studies were conducted at 25°C, 45°C and 65°C by shaking 0.03 g of nano-crystalline MgO with 50 ml of dye solution in the concentration range of 2×10^{-4}–1×10^{-4} M for the equilibrium contact time. After the sorption experiment, the mixture was centrifuged, and the residual dye concentration in the supernatant was spectrophotometrically determined using the calibration curves. Adsorption isotherms were determined by shaking 0.03 g of MgO (0.6 g/l) with 50 ml of dye solution at concentrations ranging from 2×10^{-4} to 1×10^{-4} M, and the solution was adjusted to pH 5 with dilute HCl for equilibrium. The solutions were thermostated at different temperatures (25°C, 45°C and 65°C). After shaking, the supernatant solution was separated from the MgO precipitate by filtration. The remaining concentrations of BPB dye in the solution were spectrophotometrically determined by monitoring the absorbance at λ_{max} 480. Fig. 1 shows the molecular structure of BPM. In all experiments, the difference between the initial dye concentration (C_o) and the equilibrium concentration (C_e) was calculated and used to calculate the adsorptive capacity (q_e) as follows: where V is the total volume (in litre) of the dye solution (l); m is the mass of the MgO adsorbent used (g); and C_o and C_e are the initial and residual molar concentrations (mol) of the dye, respectively.

3. Results and discussion

3.1. Structural characterization by atomic force microscopy and X-ray diffraction

AFM micrographs in 2D and 3D were investigated by the NT-MDT solver next device. Fig. 2a shows the 2D and 3D AFM images of nano-porous 1×1 μm^2 MgO. The analysis of the grain size was performed by Image Analyzer software attached to the solver next device. The mean grain size of the nano-clusters was 61.967 nm.

The X-ray diffraction pattern presented in Fig. 2b shows the nano-crystalline MgO in powder form for pure MgO and MgO of different concentrations. Different peaks for MgO appeared at 2θ° values of 36.8675, 42.8551, 62.1837, 74.5616 and 78.4680, which correspond to (111), (200), (220), (311) and (222) reflections, respectively, according to JCDPS card No. 89-4248 [32]. X-ray diffraction results confirmed that MgO was the only dominant phase, and no other phases appeared. The preferred orientation of MgO for both pure MgO and the MgO with the dyes are along the (200) plane. XRD patterns revealed that pure MgO and MgO with the dyes are a cubic structure. Even so, the diffraction peak intensity for pure MgO is higher than that of MgO with the dyes. This decreasing peak intensity can be attributed to adsorbents of the dyes inside the porous MgO. The lattice constants, a, for pure MgO and MgO with the dyes were obtained from the interplaner spacing of the d_{hkl} value of the (200) and (220) peaks using the following equation [33]:

$$d_{hkl} = \frac{a}{\sqrt{h^2 + k^2 + l^2}} \tag{1}$$

The mean values of the calculated lattice constants, a, for pure MgO and MgO with the dyes were 4.2180 Å and 4.2299 Å, respectively. Clearly, parameter a for MgO with the dye is larger than of pure MgO which can be interpreted as a distortion of the MgO crystal under the effect of absorbing dye. The obtained data for parameter a is in good agreement with reported value on JCDPS card No. 89-4248, which is 4.2109 Å. The crystallite size of pure MgO and MgO with the dye can be calculated depending on the full width at half maximum (FWHM) and the diffraction angle, θ, via Scherrer's equation [34]:

$$D = \frac{0.9\lambda}{\beta\cos\theta} \tag{2}$$

where β is the full-width at half maximum for the recorded peaks of the XRD peak appearing at the diffraction angle, θ.

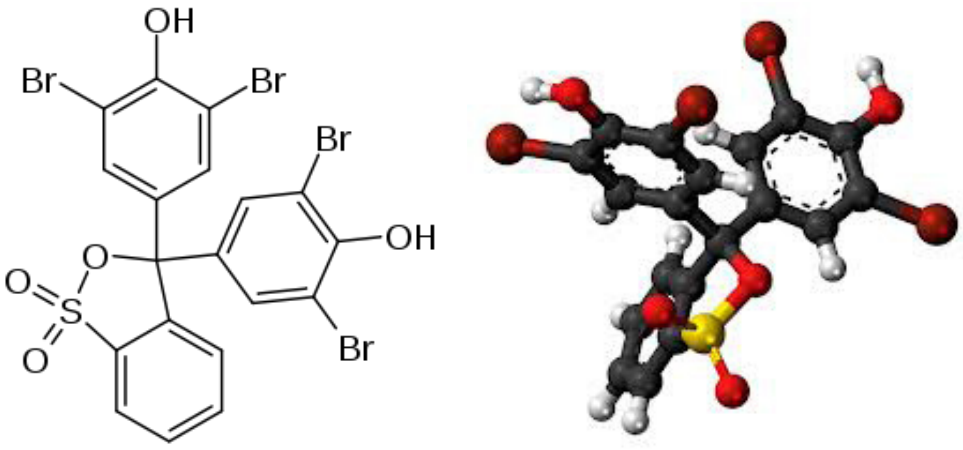

Fig. 1. Molecular structure of Bromophenol blue dye.

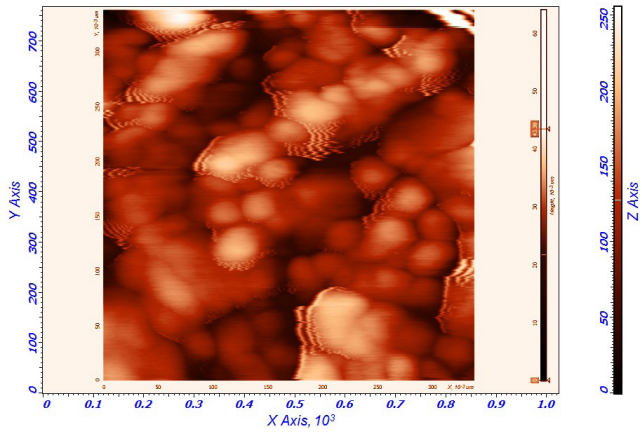

Fig. 2a. 2D AFM micrographs of pure nano-porous MgO of 1×1 μm².

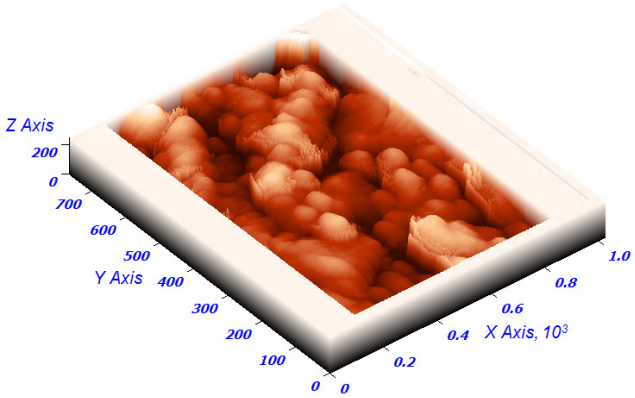

Fig. 2b. 3D AFM micrographs of pure nano-porous MgO of 1×1 μm².

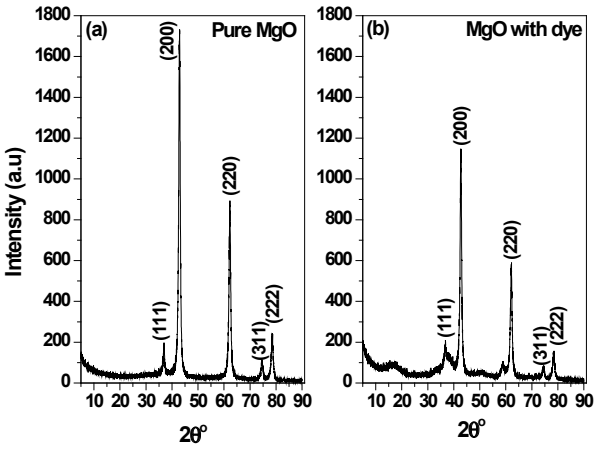

Fig. 2. (a&b). X-ray diffraction of pure MgO and MgO after removal of BPM dye.

The crystallite size was calculated for all the recorded diffraction peaks. The mean crystallite sizes of pure MgO and MgO with the dyes were 13.157 nm and 12.614 nm, respectively. Clearly, the grain size of MgO with the dye is less than that of pure MgO because of dye absorption. Depending on the values of β, θ and D, it is possible to calculate the dislocation density, δ, and crystal strain, ε, for the studied materials as follows [35–39]:

$$\delta = \frac{n}{D^2} \tag{3}$$

$$\varepsilon = \frac{\beta \cos\theta}{4} \tag{4}$$

where n is taken as unity at a minimum dislocation density. A dislocation can be defined as a crystallographic defect or irregularity within a crystal structure. The presence of dislocations strongly influences many of the properties of materials [35]. The values of the dislocation density, δ, and crystal strain, ε, for pure MgO and MgO with the dyes were 5.794×10^{-3} nm^{-2} and 6.405×10^{-3}, respectively, whereas the strain values for pure MgO and MgO with the dyes were 2.637×10^{-3} and 2.766×10^{-3}, respectively.

3.2. Effect of particle size on BPB removal

Variations in particle size can influence the chemical behaviour of MgO. The surface area of MgO increases with increasing particle size, and the adsorption rate is directly proportional to the surface area [40]. Thus, based on the surface area, compared with the coarser fractions, finer grain fractions will have a higher adsorption potential.

The efficiency of different particle sizes (10–200 mesh) on the removal of 50 ml of 2×10^{-4} MBPM dye from aqueous solution using 0.03 gm of MgO was studied at pH 5 for a shaking time 30 min at 25 ± 1°C. The removal of BMP dye was found to increase as the sorbent particle size decreased from 200 to 10 mesh (Fig. 3). Hence, MgO with a particle size of 35 mesh was chosen for further experiments.

3.3. Effect of MgO dosage on adsorption

The adsorption of BPB dye as a function of the amount of MgO at pH 5 was investigated. The MgO concentration was varied from 0.005 to 0.1 g/50 ml for the 2×10^{-4} M dye solution and equilibrated for 30 min. Adsorption of the dye increased with increasing adsorbent dosage, and equilibrium was established with 0.03 g of the sorbent (Fig. 4). For this purpose, the volume/mass of the adsorbent (V/m) was plotted as a function of q_e. The optimum MgO amount for maximum dye removal was 0.6 g/l for an initial dye concentration of 2×10^{-4} M. The removal efficiency and mechanism have been previously demonstrated [41].

3.4. Effect of shaking time

Adsorption of a fixed concentration of BPB dye at 2×10^{-4} M on MgO was studied as a function of shaking time to determine the equilibration time for maximum adsorption (Fig. 5). The residual dye concentration in the supernatant solution at a selected shaking time was measured. In total, 30 min was enough for adsorption equilibrium for the tested dye. This revealed that MgO is a good adsorbent with fast kinetics for removal of BPB dye compared with other previously suggested adsorption materials, which take a much longer time, as indicated in Table 2.

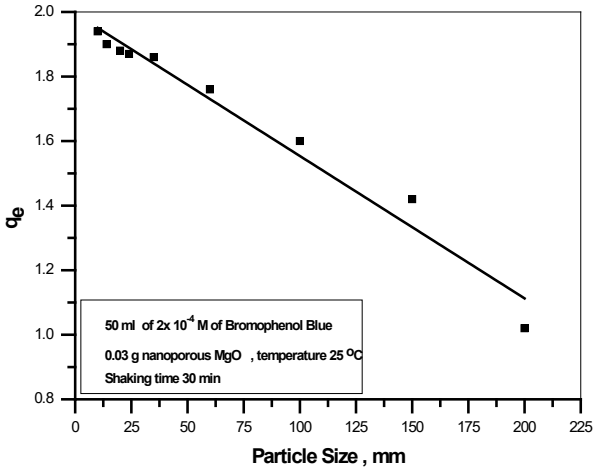

Fig. 3. Effect of particle size on removal of BPM dye.

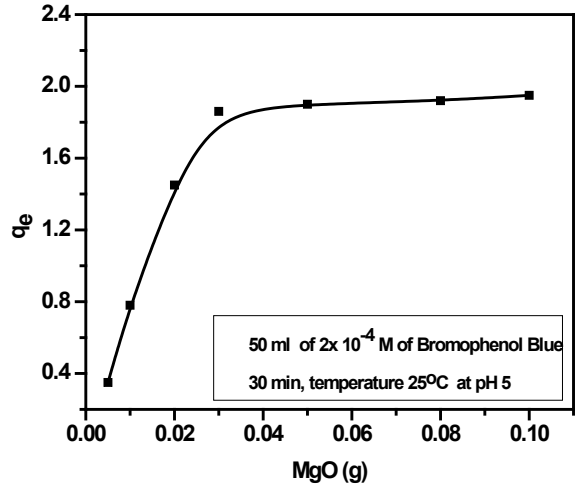

Fig. 4. Effect of MgO dosage on removal of BPM dye.

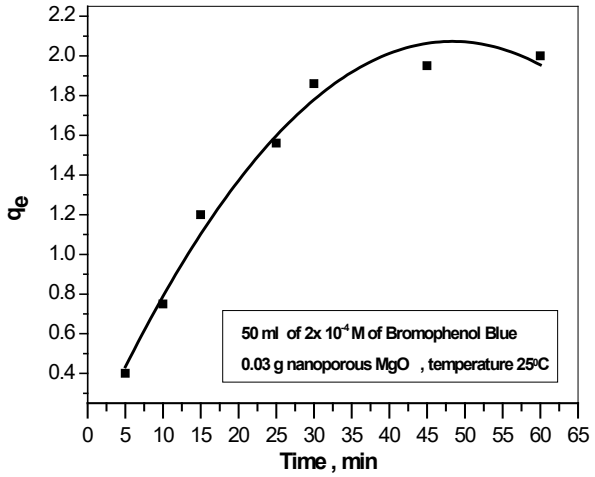

Fig. 5. Effect of shaking time on removal of BPM dye by nano crystalline MgO.

Table 2
Summary of isotherm parameters for the sorption of BPM on the synthesized nano-crystalline MgO

Langmuir			
	25°C	45°C	65°C
q_m	219	152.4	71.12
K_a	5.34	3.86	2.66
R^2	0.953	0.999	0.991
Freundlich			
N	0.847	0.751	0.735
K_f	1.096	2.108	2.356
R^2	0.996	0.994	0.9969

3.5. Effect of pH

The effect of pH on the removal of BPB dye by MgO is shown in Fig. 6. Sorption at different pH values was conducted by adjusting the pH of the dye solution at different values with HCl or NaOH before treatment with MgO. Adsorptive capacity of the BMP dye was studied at a pH range from 2 to 10 as shown in Fig. 6. The maximum uptake was obtained at pH 5. The obtained pH is suitable for waste treatment plants without further addition of chemicals or any side effects on the pH of the effluent after the treatment process. These results agree with the effective pH obtained by other workers for removal of some reactive dyes by metal hydroxide adsorbate sludge [42].

3.6. Effect of dye concentration

The experimental results of adsorption of BPM on MgO at various initial concentrations (2×10^{-4} to 0.04×10^{-4} M) are shown in Fig. 7. The percent adsorption decreased with increasing initial dye concentration; however, the actual amount of dye adsorbed per unit mass of MgO increased with increasing dye concentration. The amount of dye adsorbed increased from 13.39 mg/g at 0.04×10^{-4} M to 124.61 mg/g at a concentration of 2×10^{-4} M. The results indicate that the adsorption is dependent on the initial concentration of the dye. However, at high concentration, the available sites for adsorption decrease, and the available dye molecules increase; hence, the percentage removal of dye decreased with increasing initial concentration [43]. We suggest that this behaviour is partially due to saturation of the available sites for adsorption at a high dye concentration and also suggests possible monolayer coverage of the BPM on the MgO surface.

3.7. Effect of temperature

As the temperature was increased from 25–65°C, the percentage dye removal increased. Enhanced adsorption of BPM dye with temperature may be due to the increased mobility of dye molecules and the enlargement of pore sizes due to activated diffusion (Fig. 8). The latter is expected to widen and deepen pores, thereby creating more surface area for adsorption. Similar results have been reported by other researchers [43].

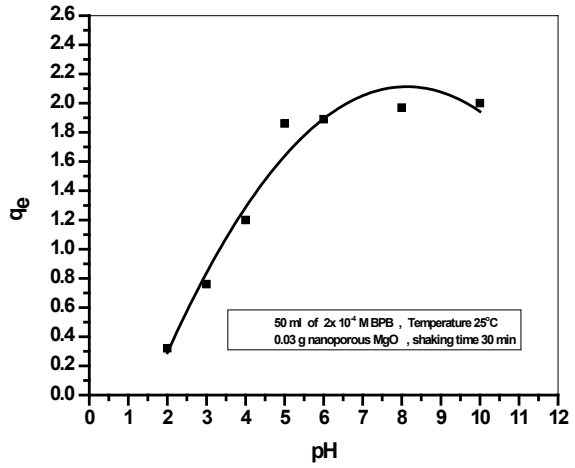

Fig. 6. Effect of pH textile waste water contained BMP dye on efficiency removal of MgO.

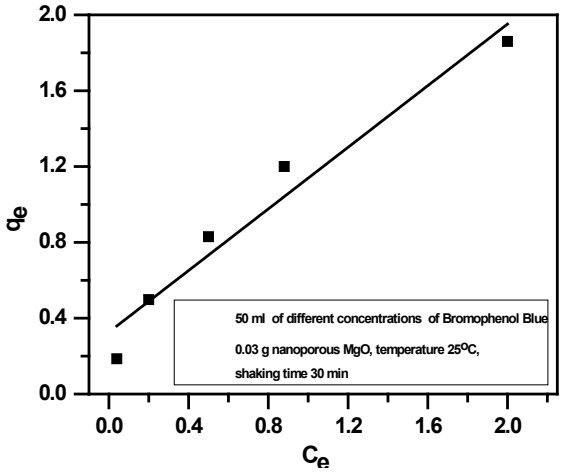

Fig. 7. Effect of different concentrations of BPM on uptake of MgO.

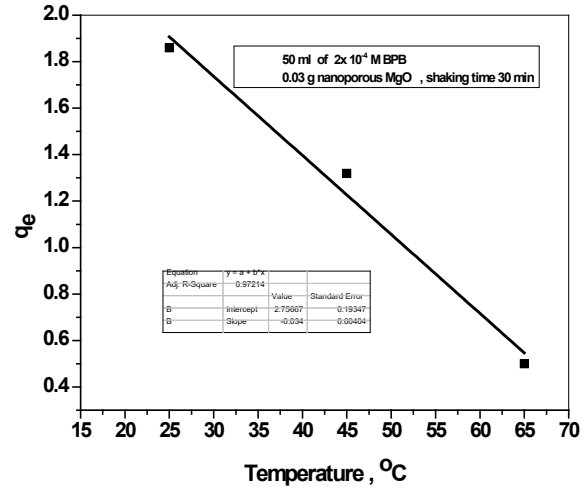

Fig. 8. Effect of temperature on removal of BPM by MgO.

3.8. Adsorption isotherms

The adsorption isotherms of the BPB dye on MgO show the relationship between the amount of adsorbed dye per weight of adsorbent (q_e) and the equilibrium concentration (C_e) at two different temperatures. Evidently, the adsorption of BPB dye on MgO decreases with an increase in temperature, indicating that the process is exothermic. Linear plots of the Langmuir model (C_e/q_e vs. C_e) are shown in Fig. 9. The maximum adsorption capacities ($Q°$) and the b constants were calculated from the slope and interception of the Langmuir plots, respectively, using the equation:

$$\frac{C_e}{q_e} = \frac{1}{q_m}C_e + \frac{1}{K_a q_m} \tag{5}$$

The linear plots of the Freundlich model (log q_e vs log C_e) are shown in Fig. 10. The Freundlich constants (n and KF) were calculated from the slope and intercept of the Freundlich plots, respectively, using the equation:

$$\log q_e = \log K_f + \frac{1}{n}\log C_e, \tag{6}$$

All calculated constants obtained from both models are listed in Table 2.

3.9. Thermodynamic studies

The free energy change ($\Delta G°$), enthalpy change ($\Delta H°$) and entropy change ($\Delta S°$) were evaluated using the following equations:

$$\Delta G° = -RT\ lnKa \tag{7}$$

$$ln(Ka_2/Ka_1) = -\Delta H°/R\ (1/T_2 - 1/T_1) \tag{8}$$

$$\Delta G° = \Delta H° - T\Delta S° \tag{9}$$

where R is the universal gas constant (8.314 J K^{-1}·mol^{-1}), and T (K) is the temperature. The results are shown in Table 3. The enthalpy change ($\Delta H°$) of adsorption of BPB dye by MgO was –56.5. This indicates that the adsorption proceeds via an exothermic process. Negative $\Delta G°$ values show a spontaneous adsorption process, and positive $\Delta S°$ values indicate the affinity of the adsorbent for the dye.

3.10. Adsorption mechanism

To investigate the mechanism of dye adsorption on MgO nanoparticles, pseudo-first-order and pseudo-second-order models were adopted. Massimiliano Fabbricino and Ludovico Pontoni (2016) [44] used shrimp shells as a solid adsorbent to remove direct dyes from wastewater. The authors found that the second-order kinetic equation and the Langmuir isotherm can simulate the process and that the removal process is due to parallel adsorption of dye molecules on the residues. Franco et al. [45] stated that ionic liquid played a crucial role in the separation of their target analyses, and they employed solid phase extraction (SPE) with conventional C18 and cation–exchange cartridges. The experimental adsorption isotherms for four anionic dyes (Acid Blue 25, Acid Yellow 99, Reactive Yellow 23 and Acid

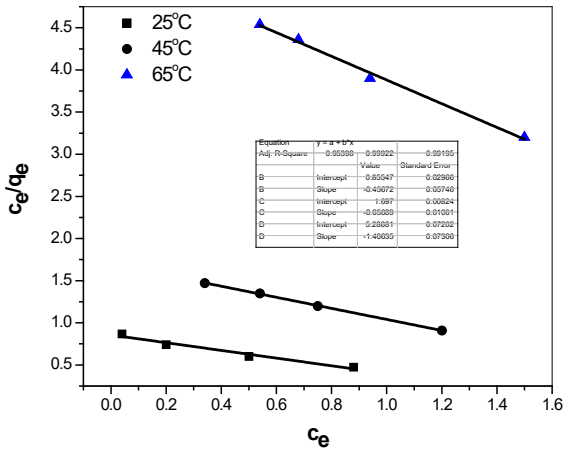

Fig. 9. Langmuir model for the sorption of BPM by synthesized nano crystalline MgO.

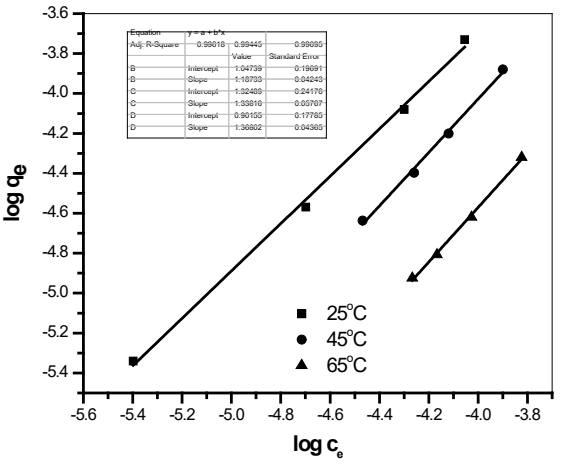

Fig. 10. Freundlich model for the sorption of BPM by synthesized nano crystalline MgO.

Table 3
Thermodynamic parameters for adsorption of BPM on the synthesized nano-crystalline MgO

Temp. K	$\Delta G°$ KJ mol^{-1}	$\Delta H°$ KJ mol	$\Delta S°$ KJ mol^{-1} K^{-1}
298	–414.95	–56.5	–0.120
318	–334.56		–0.087
338	–242.33		–0.055

Blue 74) on cationized cotton were analysed using a multilayer adsorption model by Khalfaoui et al. [46]. For this purpose, the double-layer model showed the best fit with a high correlation coefficient. This method allowed an estimation of all the mathematical parameters in the model. Physicochemical variables, including the chemical potential, the adsorption energy, and the anchorage number, were calculated. The removal of some reactive dyes (RY-145, RR-194 and RB-B) from textile wastewater effluents using Sorel's cement was described by Hassan et al. [43]. The dye adsorption equilibrium data fit well to the Langmuir isotherm but not to the Freundlish isotherm. The adsorption isotherm indicates that the adsorption capacities are 107.67, 120.89 and 103.14 mg dye per gram of Sorel's cement for RY-145, RR-194 and RB-B reactive dyes, respectively. The adsorption isotherms, including the Langmuir constants ($Q°$ and b) and Frendlich constants (KF and n), for the dyes decreased with an increase in temperature. The values for enthalpy change (ΔH) for RY-145, RR-194 and RB-B dyes were –146.96, –49.23 and –264.86 kJ mol^{-1}, respectively, indicating that the removal process is exothermic. The removal of malachite green dye (MG) from aqueous solution was studied using organically modified hydroxyapatite by El-Zahhar and Awwad [47]. Hydroxyapatite (HAP) was organically modified with different concentrations of the organic surfactant, ethylhexadecyldimethyl ammonium bromide (EHDAB). The effect of contact time, adsorbent dose, dye concentration and temperature was studied. The equilibrium uptake increased with increasing initial dye concentration in solution. The experimental isotherm data were analysed using the Langmuir adsorption isotherm model. The amount of adsorbed MG on a modified apatite was found to increase with increasing adsorbent concentration. The maximum monolayer adsorption capacity was found to be 188.18 mg/g at 30°C. A composite material was prepared by El-Zahhar et al. [48] that incorporated the clay (kaolinite) into a poly(acrylamide co-acrylic acid) through the in situ polymerization method with a cross-linker. Different factors that could affect the bromophenol blue (BPB) dye adsorption behaviour were studied, including time of contact, dye concentration and temperature. The kinetic studies revealed that the adsorption results fit the Lagergren model (pseudo-first-order reaction rate) well. The isotherm studies also showed that the adsorption data fit with the Freundlich model better than with the Langmuir isotherm model. Based on the effect of temperature, the thermodynamic parameters were calculated, and a free energy change ($\Delta G°$) value of –110.323 kJ/mol was obtained, suggesting the feasibility and spontaneous nature of the sorption reaction. Additionally, the relatively high negative value of entropy changes of $\Delta S°$ = –509.4 J mol^{-1} K^{-1} suggested the chemical nature of the sorption reaction. The amount of adsorbed dye on MgO was studied as a function of time to estimate the adsorption mechanism. The adsorption of dye with time showed that a mixing period of 30 min is optimum for attaining equilibrium with respect to MgO. Different kinetic models were applied on the obtained results, and the kinetic parameters were determined. The kinetic models correlate the amount of adsorbed dye with time. The Lagergren model was presented for pseudo-first-order reactions, and the rate constant (K) and the adsorption capacity (q_e) was determined. From the calculated data, we determined that the adsorption capacity, q_e, and the linear regression coefficient for the studied kinetic model did not fit with the experimental results for the adsorption of BPM on MgO. The second-order kinetic model, which describes the chemical adsorption has been described by many researchers. The results of the studied kinetic model show that experimental results for the adsorption of BPM on MgO fit and were described by the kinetic model that supports chemical adsorption. The sorption of BPM could be

favourably described by the pseudo-second-order kinetic model on MgO. This finding refers to the participation of chemical adsorption within the adsorption mechanism for BPM on MgO. Several earlier researchers have also shown that the pseudo-second-order model fits well for describing the adsorption process [49–51]. The Dubinin–Radushkevich (D–R) adsorption isotherm model was studied, which describes adsorption on porous solid surfaces. The calculated mean adsorption free energy (ES) from the D-R model for the adsorption of BPM on MgO was found to be 6.83 kJ/mol. This values shows that physical adsorption is a participating mechanism. The pseudo-second-order model suggests that the adsorption depends on the adsorbate and the adsorbent and involves a chemisorption process in addition to physisorption [49]. The net conclusion from the obtained data are that the mechanism of adsorption of BPM on MgO includes both physical and chemical adsorption.

3.11. Spectroscopic studies

3.11.1. Diffuse reflectance (DR)

Diffuse reflectance spectroscopy (DR) is a rapid survey technique that locates the main regions of absorption and provides information on the energy, width, and intensity of absorption bands [50]. In this case, nano-powder samples (pure MgO and MgO with the dye) as a pellet of a specific thickness (1.5 mm) was used for the diffuse reflectance measurements.

The measured diffused reflectance spectra of pure MgO and MgO with the dye are shown in Fig. 11. The DR of pure MgO was larger than the DR of MgO with the dye. Additionally, the diffuse reflectance spectrum of MgO showed two minimum peaks at 556 nm (2.230 eV) and 244 nm (5.08 eV); however, for MgO with the dye, there were three weak peaks at wavelengths of 616 nm (2.013 eV), 348 nm (3.56 eV) and 250 (4.96 eV). McKenna et al. [51] studied the UV-VIS diffuse reflectance spectra of compaction MgO nano-powders. They found that there are two absorption features (bands) in the range of 4.0–5.5 eV. They attributed these changes (with the help of complementary first-principles calculations) to the excitation of nano-crystal interfaces [52]. They concluded that the photons with low energy, e.g., 4.6 eV, excite electrons not only at MgO surfaces, as previously believed, but also at interfaces inside the nano-powder. This is the first experimental evidence for the emergence of new electronic states that arise from the contact area between nano-crystals [53,54]. Our results are in good agreement with the reported data by McKenna et al. [51] regarding the presence of a new absorption range inside MgO nano-powders at low photon energy. The absorption of the dye on nano-porous MgO led to new absorption energy bands that differed from that on pure MgO. Additionally, these changes in absorption bands lead to changes in XRD parameters, such as the grain size, the dislocation density and the strain of MgO nano-crystals. We concluded that the dye absorbed inside MgO leads to the creation of the defects and thus the distortion of the MgO crystals.

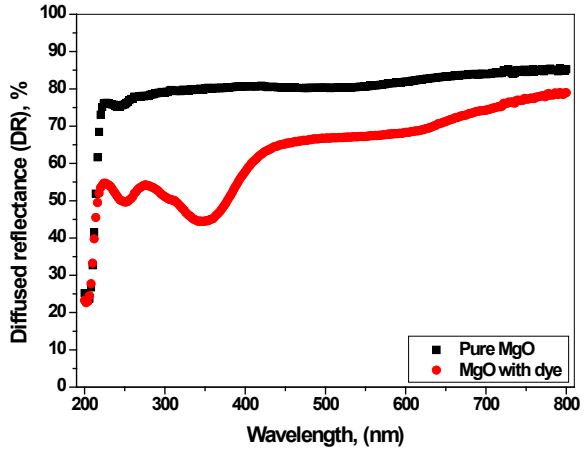

Fig. 11. Diffused reflectance of pure MgO and MgO with BPM dye.

4. Antibacterial activity of MgO for *B. subtilus* and *E. coli*

The viabilities of *B. subtilus* and *E. coli* were determined when exposed for different times to MgO. The surviving colonies were counted by eye. From the data obtained, we found that control sample did not decrease in CFU cells for the different times; however, the best inhibitory time for MgO against 10^8 CFU/mL of *B. subtilus* and *E. coli* was

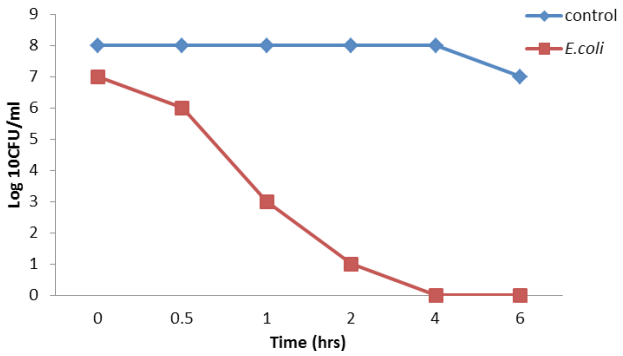

Fig. 12. a. Antimicrobial effect of MgO against of *E.coli* (10^8 cfu/ml), at different times. Control sample is *E. coli* without MgO.

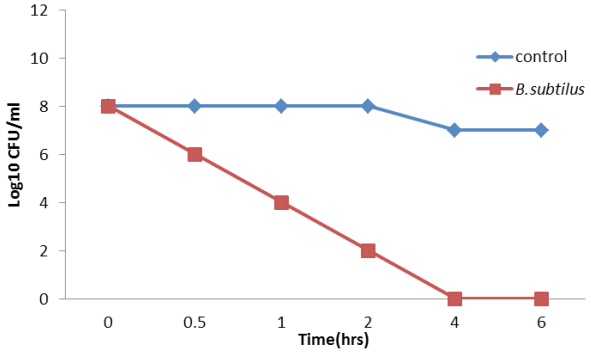

Fig. 12. b. Antimicrobial effect of MgO against of *B. subtilus* (10^8 cfu/ml), at different times. Control sample is *B. subtilus* without MgO.

4 h for 0.5 g of MgO, which was required to kill all cells as shown in Figs. 12a,b. Additionally, TEM was conducted for MgO with and without *B. subtilus* and *E. coli* as shown in Figs.13a–c.

Fig. 13. a. TEM for antimicrobial effect of MgO against of *B. subtilus* (10^8 cfu/ml),or *E. coli* (10^8 cfu/ml) after 2 h.

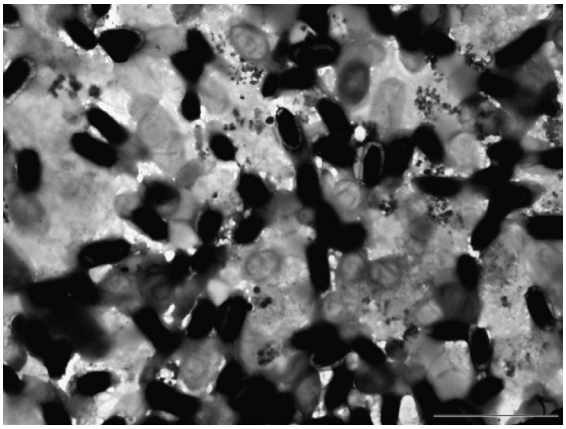

Fig. 13. b. TEM for antimicrobial effect of MgO against of *B. subtilus* (10^8 cfu/ml), at zero times.

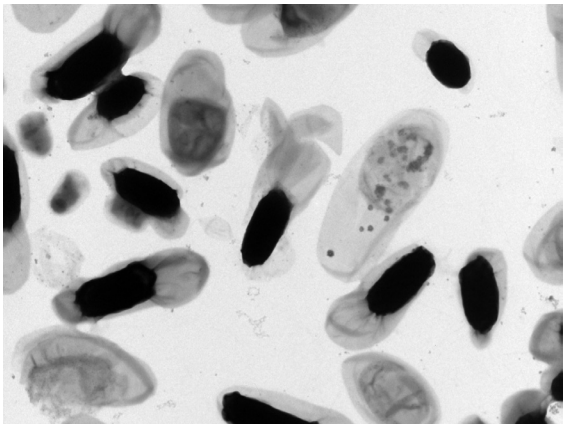

Fig. 13. c. TEM for antimicrobial effect of MgO against of *E. coli* (10^8 cfu/ml) at zero time.

5. Conclusions

Nano-crystalline MgO was prepared by the co-precipitation method, and the final MgO was calcined at 500°C. XRD and AFM micrographs supported the nano-structure of the studied MgO. The crystalline size was calculated by the Scherrer's equation to be 13.175 nm, and the nano-cluster size of MgO by AFM analysis was 61.967 nm. MgO was effectively used for the removal of BPB dye from wastewater. The adsorbed amount of the BPB dye increased with an increase in the contact time and adsorbent dosage, reaching a maximum equilibrium for 10^{-4} M of dye at 30 min and for 0.02 g adsorbent. The adsorbed amount of dye decreased with increasing temperature. The diffused reflectance measurements and analysis revealed the presence of new absorption bands after absorbing the dye, which is different than the pure MgO at a lower photon energy. The dye absorbance affects the crystal structure and the absorption bands of the dye on MgO. It was concluded that the absorbed dye inside MgO leads to the creation of new defects and thus distortion of the MgO crystals.

Acknowledgments

The authors extend their appreciation to the Deanship of Scientific Research at King Khalid University for funding this work through the Project for Group Research under grant number G.R.P.1/23/38.

References

[1] G. McMullan, C. Meehan, A. Conneely , N. Kirby, T. Robinson, P. Nigam, I.M. Banat, R. Marchant, W.F. Smyth, Microbial decolourisation and degradation of textile dyes, Appl. Microbiol. Biotechnol., 56 (2001) 81–87.

[2] C.I. Pearce, J.R. Lloyd, J.T. Guthrie, The removal of color from textile wastewater using whole bacterial cells, a review : Dyes Pigments, 58 (2003) 179–196.

[3] E.Y. Ozmen, M. Sezgin, A. Yilmaz, M. Yilmaz, Synthesis of beta-cyclodextrin and starch based polymers for sorption of azo dyes from aqueous solutions, Bioresour. Technol., 99 (2008) 526–531.

[4] G. Moussavi, M.Mahmoudi, Removal of azo and anthraquinone reactive dyes from industrial wastewaters using MgO nanoparticles, J. Hazard. Mater., 168 (2009) 806–812.

[5] R. Han, D. Ding, Y. Xu, W. Zou, Y. Wang, Y. Li, L. Zou, Use of rice husk for the adsorption of congo red from aqueous solution in column mode, Bioresour. Technol., 99 (2008) 2938–2946.

[6] M. Rezaei, M. Khajenoori, B. Nematollahi, Synthesis of high surface area nanocrystalline MgO by Pluronic P123 triblock copolymer surfactant, Powder Technol., 205 (2011) 112–116.

[7] Z. Jiabin, Y. Siliang, Y. Jiaguo, Facile fabrication of mesoporous MgO microspheres and their enhanced adsorption performance for phosphate from aqueous solutions, Colloids Surf. A., 379 (2011) 102–108.

[8] N.S. Awwad, A.M. Alshahrani, K.A. Saleh, M.S. Hamdy, A novel method to improve the anticancer activity of natural-based hydroxyapatite against the liver cancer cell line HepG2 using mesoporous magnesia as a micro-carrier, Molecules, 22 (2017) 1947.

[9] M.S. Hamdy, N.S. Awwad, A.M. Alshahrani, Mesoporous magnesia: Synthesis, characterization, adsorption behavior and cytotoxic activity, Mater. Design, 110 (2016) 503–509.

[10] J. Sawai, H. Kojima, H. Igarashi, A. Hashimoto, S. Shoji, T. Sawaki, A. Hakoda, E. Kawada, T. Kokugan, M. Shimizu, Antibacterial characteristics of magnesium oxide powder, World J. Microb. Biot., 16 (2000) 187–194.

[11] O. Yamamoto, J. Sawai, T. Sasamoto, Effect of CaO doping on antibacterial activity of ZnO powder, J. Inorg. Mater., 2 (2000) 451–454.
[12] O.B. Koper, J.S. Klabunde, G.L. Marchin, K.J. Klabunde, P. Stoimenov, L. Bohra, Nanoscale powders and formulations with biocidal activity toward species and vegetative cells of bacillus species, viruses, and toxins, Curr. Microbiol., 44 (2002) 49–55.
[13] P.K. Stoimenov, R.L. Klinger, G.L. Marchin, K.J. Klabunde, Metal oxide nanoparticles as bactericidal agents, Langmuir, 18 (2002) 6679–6686.
[14] G.W. Wagner, O.B. Koper, E. Lucas, S. Decker, L.J. Klabunde, Reactions of VX, GD, and HD with nanosize CaO: Autocatalytic dehydrohalogenation of HD, J. Phys. Chem. B, 104 (2000) 5118–5123.
[15] G.W. Wagner, L.R. Procell, R.J. O'Connor, S. Munavalli, C.L. Carnes, P.N. Kapoor, K.J. Klabunde, Reactions of VX, GB, GD, and HD with nanosize Al_2O_3. Formation of aluminophosphonates, J. Am. Chem. Soc., 123 (2001) 1636–1644.
[16] M.E. Martin, R.M. Narske, K.J. Klabunde, Mesoporous metal oxides formed by aggregation of nanocrystals, Micropor. Mesopor. Mater., 83 (2005) 47–50.
[17] G.K. Prasad, P.V.R.K. Ramacharyulu, J.P. Kumar, K. Ganesan, B. Singh, Comparative evaluation of various sorbent decontaminants against sulphur mustard, J. Sci. Ind. Res., 71 (2012) 205–209.
[18] T.H. Mahati, G.K. Prasad, B. Singh, J. Acharya, A.R. Srivastava, R. Vijayaraghavan, Nanocrystalline zinc oxide for the decontamination of sarin, J. Hazard. Mater., 165 (2009) 928–932.
[19] C. Bisio, F. Carniato, C. Palumbo, S.L. Safronyuk, M.F. Starodub, A.M. Katsev, L. Marchese, M. Guidotti, Nanosized inorganic metal oxides as heterogeneous catalysts for the degradation of chemical warfare agents, Catal. Today, 277 (2016) 192–199.
[20] J.P. Kumar, G.K. Prasad, P.V.R.K. Ramacharyulu, P. Garg, K. Ganesan, Mesoporous CuO-ZnO binary metal oxide nanocomposite for decontamination of sulfur mustard, Mater. Chem. Phys., 142 (2013) 484–490.
[21] N.E. Zander, E. Kowalski, A.M. Rawlett, J.A. Orlicki, Decontamination of chemical agent simulant by nanometal oxides. Army Res. Lab. (2007). Report No. ARL-TR-4133, 18 pages.
[22] G.K. Prasad, P.V.R.K. Ramacharyulu, J.P. Kumar, A.R. Srivastava, B. Singh, Photocatalytic degradation of paraoxon-ethyl in aqueous solution using titania nanoparticles film, Thin Solid Films, 520 (2012) 5597–5601.
[23] A.T. Vu, S. Jiang, K. Ho, J.B. Lee, C. H. Lee, Mesoporous magnesium oxide and its composites: preparation, characterization, and removal of 2-chlorothyl ethyl sulfide, Chem. Eng. J., 269 (2015) 82–93.
[24] G.W. Wagner, P.W. Bartram, O. Koper, K.J. Klabunde, Reactions of VX, GD and HD with nanosize MgO, J. Phys. Chem., 103 (1999) 3225–3228.
[25] B. Maddah, H. Chalabi, Synthesis of MgO nanoparticales and identification of their destructive reaction product by 2-chloroethyl ethyl sulfide, J. Nanosci. Nanotechnol., 8 (2012) 157–164.
[26] L. Zhang, Y. Jiang, Y. Ding, N. Daskalakis, L. Jeuken, A.J. O'Neill, D.W. York, Mechanistic investigation into antibacterial behavior of suspensions of ZnO nanoparticles against *E. coli*, J. Nanopart. Res., 12 (2010) 1625–1636.
[27] J. Vidic, S. Stankic, F. Haque, D. Ciric, R. Le Goffic, A. Vidy, J. Jupille, B. Delmas, Selective antibacterial effects of mixed ZnMgO nanoparticles, J. Nanopart. Res., 15 (2013) 1595–1604.
[28] O.B. Kopler, J.S. Hlabunde, G.L. Marchin, K.J. Klabunde, P. Stoimenov, L. Bohra, Nanoscale powders and formulations with biocidal activity toward spores and vegetative cells of Bacillus species, viruses, and toxins, Curr. Microbiol., 44 (2002) 49–55.
[29] Z.X. Tang, B.F. Lv, MgO nanoparticles as antibacterial agent: preparation and activity, Braz. J. Chem. Eng., 31 (2014) 591–601.
[30] E. Scallan, R.M. Hoekstra, F.J. Angulo, R.V. Tauxe, M.-A. Widdowson, S.L. Roy, Foodborne illness acquired in the United States--major pathogens, Emerg. Infect Dis., 17 (2011) 7–15.
[31] K. Ganapathi Rao, C.H. Ashok, K. Venkateswara Rao, C.H. Shilpa Chakra, Structural properties of MgO nanoparticles: synthesized by co-precipitation technique, Int. J. Sci. Res., (IJSR), (2014) 43–46. ISSN: 2319-7064.
[32] International Centre for Diffraction Data. JCDPS, PCPDFWIN, V.2.3; 2002, No. (89-4248).
[33] G. Kittel, Introduction to Solid State Physics, fifth edition, John Wiley and Sons, New York,1976.
[34] B.D. Cullity, Elements of X-ray Diffraction, Addison-Wesley, Massachusetts, 1956.
[35] W.D. Callister, Materials Science and Engineering—An Introduction, John-Wiley and Sons, New York, 1997.
[36] D.P. Padiyan, A. Marikini, K.R. Murli, Influence of thickness and substrate temperature on electrical and photoelectrical properties of vacuum-deposited CdSe thin films, Mater. Chem. Phys., 78 (2002) 51.
[37] K.R. Murali, A. Kalaivanan, S. Perumal, N. Neelakanda Pillai, Sol–gel dip coated CdO:Al films, J. Alloys Compd., 503 (2010) 350.
[38] C. Barret, T.B. Massalski, Structure of Metals, Pergamon, Oxford, 1980.
[39] C. Aydin, H.M. El-Nasser, F. Yakuphanoglu, I.S. Yahia, M. Aksoy, Nanopowder synthesis of aluminum doped cadmium oxide via sol–gel calcination processing, J. Alloys Compd., 509 (2011) 854–858.
[40] A.W. Adamson, Physical chemistry of surfaces, John Wiley and Sons, London, 1976, 698.
[41] International Centre for Diffraction Data. JCDPS, PCPDFWIN, v. 2.3; 2002, No. (89-4248).
[42] S.S.M. Hassan, N.S. Awwad, A.H.A. Aboterika, Removal of chromium(VI) from wastewater using Sorel's cement, J. Radioanal. Nucl. Chem., 269 (2006) 135–140.
[43] S.S.M. Hassan, N.S. Awwad, H.A.A. Awaad, Removal of synthetic reactive dyes from textile wastewater by Sorel's cement, J. Hazard. Mater., 162 (2009) 994–999.
[44] M. Fabbricino, L. Pontoni, Use of non-treated shrimp-shells for textile dye removal from wastewater, J. Environ. Chem. Eng., 4 (2016) 4100–4106.
[45] J.H. Franco, B.E. Silva, M.V.B. Zanoni, Using ionic liquid combined with HPLC-DAD to analyze semi-permanent hair dyes in commercial formulations, Anal. Methods, 7 (2015) 1115.
[46] M. Khalfaoui, M.H. Baouab, R. Gauthier, A.B. Lamine, Statistical physics modelling of dye adsorption on modified cotton, Adsorpt. Sci. Technol., 20(1) (2002) 17–31.
[47] A.A. El-Zahhar, N.S. Awwad, Removal of malachite green dye from aqueous solutions using organically modified hydroxyapatite, J. Environ. Chem. Eng., 4 (2016) 633–638.
[48] A.A. El-Zahhar, N.S. Awwad, E. Katori, Removal of Bromophenol blue dye from industrial waste water by synthesizing polymer-clay composite, J. Mol. Liq., 199 (2014) 454–461.
[49] G.L. Dotto, L.A.A. Pinto, Adsorption of food dyes acid blue 9 and food yellow 3 onto chitosan: stirring rate effect in kinetics and mechanism, J. Hazard. Mater., 187 (2011) 164–170.
[50] S. Saravanabhavan, K.J. Sreeram, J.R. Rao, B.U. Nair, The use of toxic solid waste for the adsorption of dyes from waste streams, J. Chem. Technol. Biotechnol., 82 (2007) 407–413.
[51] P.M. Keith, K. David, S. Andreas, S. Nicolas, G. Niranjan, V. S. Peter, D. Oliver, optical properties of nanocrystal interfaces in compressed MgO nanopowders, ACS Nano, 5 (2011) 3003–3009.
[52] L. Wang, A. Wang, Adsorption behaviors of Congo red on the N, O-carboxymethyl-chitosan/montmorillonie nanocomposite, Chem. Eng. J., 143 (2008) 43–50.
[53] B.J. Wood, Ph.D. thesis, University of Newcastle - UPON - TYNE. (Tokyo) 1970.
[54] L. Xiong, Y. Yang, J. Mai, W. Sun, C. Zhang, D. Wei, Q. Chen, J. Ni, Adsorption behavior of methylene blue onto titanate nanotubes, Chem. Eng. J., 156 (2010) 313–320.